International Journal of Thermofluid Science and Technology (2020)
Volume 8, Issue 2, Paper No. 080202
https://doi.org/10.36963/IJTST.2021080202
Research Article

Simultaneous impact of magnetic and Arrhenius activation energy on the flow of Casson hybrid nanofluid over a vertically moving plate.

Deepak Umrao Sarwe[1], Bandari Shanker[2], Raghawendra Mishra[3], R.S. Varun Kumar[4], M.N Raja Shekar[5].

[1]*University of Mumbai, Kalina, Santacruz East, Mumbai400098, India*
[2]*Department of Mathematics, CVR College of Engineering, Hyderabad, India*
[3]*S.B.S Government Post Graduate College, Rudrapur, Uttarakhand, India*
[4]*Department of Mathematics, Davangere University, Davangere-577007. India*
[5]*Department of Mathematics, JNTU College of Engineering, Hyderabad, India*

Received: 22 December 2020; Received in revised form: 16 March 2021; Accepted: 23 March 2021; Published online 03 April 2021

Abstract

The present study deals with the Blasius and Sakiadis flow of Casson hybrid nanoliquid over a vertically moving plate under the influence of magnetic effect and Joule heating. Here, we considered Silver and Copper as nanoparticles suspended in 50% Ethylene-Glycol (EG) as base fluid. Further, the Arrhenius activation energy and convective boundary conditions are taken into the account. The set of PDEs of the current model are converted into ODEs by using suitable similarity variables. The reduced ODEs are numerically solved with the help of RKF-45 method by adopting shooting scheme. The impact of various pertinent parameters on the fluid fields is deliberated graphically. The result outcomes reveal that, rise in values of Casson parameter diminishes the velocity gradient. The escalated values of magnetic parameter decline the velocity profile but reverse trend is detected in thermal and concentration profiles. Moreover, the augmentation in the activation energy parameter elevates the concentration profile.

Keywords: Casson hybrid nanofluid; Magnetic effect; Arrhenius activation energy; Moving plate.

1. Introduction

The thermal conductivity of the fluid is the main aspect of the heat transfer process. The base liquids namely, water, oil, and Ethylene–Glycol (EG) have low thermal conductivity. In order to enhance the thermal conductivity of base fluids, the nanosized metallic or non-metallic substances are adequately suspended in the base fluids. These kinds

Corresponding e-mail: deepak.sarve@mathematics.mu.ac.in (Deepak Umrao Sarwe)

of fluids are called as "nanofluids" which has high thermal conductivity than that of base liquids. These fluids have numerous industrial and engineering applications such as cable drawing, extrusion, glass fiber production, lubricant, hot rolling, metal spinning, chilling process, power generation, electronic devices, nuclear reactors, and transportation.

Many researchers analyzed the characteristics of fluids suspended with nanoparticles. The concept of nanofluids was initially scrutinized by Choi [1]. Hoseinzadeh et al. [2] experimentally discussed the thermophysical performance of nanoparticles. Sheikholeslami et al. [3] explored the significant aspect of ohmic heating and magnetic effect on the nanoliquid stream past an extending sheet. Hoseinzadeh et al. [4] explicated the significant investigations on the flow nature of nanoliquid through a channel. Khan et al. [5] scrutinized the effect of thermal radiation and activation energy on the flow of a nanoliquid over a rotating disk. Hoseinzadeh et al. [6] debriefed the heat transfer, laminar and turbulent stream of water-based nanoliquid through a channel. In the past decades, with the intention of improving the features of heat transfer, researchers are utilizing more than one nanoparticle in base fluid for obtaining superior thermal conductivity. The special type of nanofluid, which is synthesized by mixing more than one kind of nanoparticles in the base fluid is called as hybrid nanofluid. Recently, Mallikarjuna et al. [7] elucidated the hybrid nanoliquid stream over a stretching sheet with the impact of melting effect. Gowda et al. [8] deliberated the thermophoretic particles deposition on hybrid nanofluid flow past a moving rotating disk.

The fluids which exhibit the shear stress and shear rate dependent viscosity are categorized as non-Newtonian fluids. It is a well-known fact that, we cannot find a single specific mathematical model that can explain the important behaviour of all the different liquids involved in real world problems and also there does not exist a single non-Newtonian model that can do so. But the non-Newtonian fluids have significant industrial applications in ground water hydrology, atomic waste transfer, geothermal energy formation, transpiration cooling, oil supplies, and structure of strong lattice heat. So, there is a need for studying the behaviour of different fluids. For this reason, different rheological fluid models have been presented. Casson fluid is one of the most important non-Newtonian fluid models which has numerous applications in metallurgy, bio-engineering problems and drilling procedures. In the past years, numerous investigations were performed by many researchers on the flow, heat and mass transfer of non-Newtonian Casson liquids. The heat transfer mechanism and flow of magnetized Casson nanofluids over an extending sheet was investigated by Rasool et al. [9]. Amjad et. al [10] explained the flow of Casson nanoliquid through a curved extending surface in the existence of magnetic field. Jamshed and Aziz [11] explored the rate of heat transfer and entropy production in the flow of Casson fluid with suspended hybrid nanoparticles over a sheet. Aman et al. [12] inspected the MHD flow of Casson hybrid nanofluid in a vertical channel. A sophisticated investigation explaining the entropy generation in hybrid Casson nanofluid flow past a surface was deliberated by Ahmad and Nadeem [13].

Nomenclature

D	diffusion coefficient	ρ	density
E	dimensionless activation energy	ρC_p	heat capacitance
E_a	activation energy	θ	non-dimensional temperature profile
Ec	Eckert number	ϕ_1, ϕ_2	solid volume fractions of Nanoparticles
$f(\eta)$	dimensionless stream function	δ	temperature difference
Gr	Grashof number	σ	chemical reaction rate parameter
gr	mixed convection parameter	μ	dynamic viscosity
K	Boltzmann's constant	υ	kinematic viscosity
$K_r^{\,2}$	chemical reaction rate	χ	dimensionless concentration
k	thermal conductivity		
M	magnetic parameter	Subscripts	
m_1	velocity ratio parameter	bf	base fluid
Pr	Prandtl number	f	fluid
Re	Reynolds number	hnf	hybrid nanofluid
Sc	Schmidt number	s_1, s_2	Solid particles
(T, C)	fluid (temperature, concentration)	w	surface/wall
(u, v)	velocity components in (x, y) directions	∞	ambient

The impact of magnetic field on the flow of fluid is becoming one of the significant study topics due to its abundant applications in electric dynamo, magnetic resonance imaging, chemical engineering, levitation with the magnetic field, Maxwell coil, and stellar magnetic strength. In view of this, many researchers examined the aspects of magnetic field on the flow of various fluids past different surfaces. Prasannakumara et al. [14] examined the influence of thermal radiation and magnetic effect on the two-dimensional stream of dusty liquid past a stretching surface. Ramzan et al. [15] explained the impact of magnetic effect and slip effect on the stream of an incompressible micropolar nanoliquid caused by a rotating disk. Prasannakumara et al. [16] inspected the thermal radiation effect on the nanofluid stream over a revolving disk on taking account of convective boundary condition. Khan and Azam [17] elucidated the heat transfer and stream of nanoliquid over a permeable extending sheet with the consideration of time dependent magnetic field. Prasannakumara et al. [18] scrutinized the impact of chemical reaction, magnetic effect and radiation effect on the stream of Siskonanofluid past a sheet. Consequently, the aspect of magnetic effect on the stream of hybrid nanoliquid through an extending cylinder was examined by Christopher et al. [19]. Ahmad et al. [20] examined the behavior of the magnetic effect on the nanofluid flow at a stagnation point. Tulu and Ibrahim [21] analyzed the magnetic effect on the Casson nanoliquid flow through a cylinder. The stream of Oldroyd-B nanofluid under the influence of magnetic effect past a vertical plate was studied by Mishra et al. [22].

The minimum amount of energy essential to start the chemical reaction is defined as Activation energy. In 1889, a Swedish scientist Svante Arrhenius introduced the term activation energy. The activation energy is generally applicable in geothermal applications, oil reservoirs, food processing, chemical manufacturing, and mechanical chemistry. In regard to these significant applications, several researchers examined the nature of Arrhenius activation energy on the different liquid flows. The influence of magnetic effect with activation energy on the stream of nanoliquid caused by a spinning disk was examined by Kotresh et al. [23]. Ijaz et al. [24] analyzed the heat transfer and two-dimensional(2D) flow of a fluid past an expanded sheet in the existence of Arrhenius activation energy and Joule heating effect. Jayadevamurthy et al. [25] presented a model that significantly describes the aspects of Arrhenius activation energy in the flow of hybrid nanofluid through a rotating disk. Kumar et al. [26] elucidated the consequence of activation energy on a magnetized nanofluid stream past a stretched surface. From past decades, many researchers examined the flow features of different fluids through moving plates. Recently, Kumar et al.[27] examined the influence of shape effect in the flow of nanofluid over a moving plate. Makinde et al. [28] inspected the Blasius and Sakiadis stream of non-Newtonian fluid over a plate. The nanofluid flow past a moving plate placed in a porous medium with the influence of magnetic effect was analyzed by Anwar et al. [29].The numerical analysis was presented by Shuaib et al. [30] which indicates the nanofluid stream between the dual plates in which the upper plate moves with a constant velocity. Anuar et al. [31] explained the impact of suction and the mixed convection flow of fluid with Carbon nanotubes over a plate which is steady in motion.

The aforementioned literature survey confirms that the Blasius-Sakiadis flow of non-Newtonian Casson hybrid nanoliquid past a vertical plate with the consideration of Arrhenius activation energy and magnetic field is not yet discussed. So, we aim to explore the Blasius-Sakiadis flow of Casson hybrid nanofluid over a moving plate subjected to the magnetic field in the presence of Arrhenius activation energy. The newly formulated partial differential equations are modified into ordinary differential equations (ODEs) by employing suitable similarity transformations. The reduced ODEs are numerically solved with the help of RKF-45 method by adopting shooting scheme. Also, the graphs are presented for analyzing the effect of several parameters on the respective flow fields.

2. Formulation of the problem

Consider the incompressible Blasius-Sakiadis flow of Casson hybrid nanofluid flow through a vertical moving plate with Silver and copper nanoparticles suspended in 50% Ethylene glycol which acts as a base fluid. Here, we considered 2D laminar boundary-layer flow of a Casson hybrid nanofluid past a static and moving flat plate (Blasius-Sakiadis problem). The Flow Geometry and coordinate system is as shown in Fig.1. The equations which govern the above-described fluid flow with the influence of mixed convection, magnetic and Joule heating are given below.

$$\frac{\partial u}{\partial x}+\frac{\partial v}{\partial y}=0 \tag{1}$$

$$u\frac{\partial u}{\partial x}+v\frac{\partial u}{\partial y}=\frac{\mu_{hnf}}{\rho_{hnf}}\left(1+\frac{1}{\beta^{*}}\right)\left(\frac{\partial^2 u}{\partial y^2}\right)-\frac{\sigma_{hnf}B_0^2}{\rho_{hnf}}u+\frac{g(\rho\beta)_{hnf}(T-T_\infty)}{\rho_{hnf}} \tag{2}$$

$$u\frac{\partial T}{\partial x}+v\frac{\partial T}{\partial y}=\frac{k_{hnf}}{(\rho C_p)_{hnf}}\left(\frac{\partial^2 T}{\partial y^2}\right)+\frac{\sigma_{hnf}B_0^2}{(\rho C_p)_{hnf}}(u^2) \tag{3}$$

$$u\frac{\partial C}{\partial x}+v\frac{\partial C}{\partial y}=D_{hnf}\left(\frac{\partial^2 C}{\partial y^2}\right)-k_r^2\left(\frac{T}{T_\infty}\right)^n e^{-\frac{E_a}{KT}}\left(C-C_\infty\right) \tag{4}$$

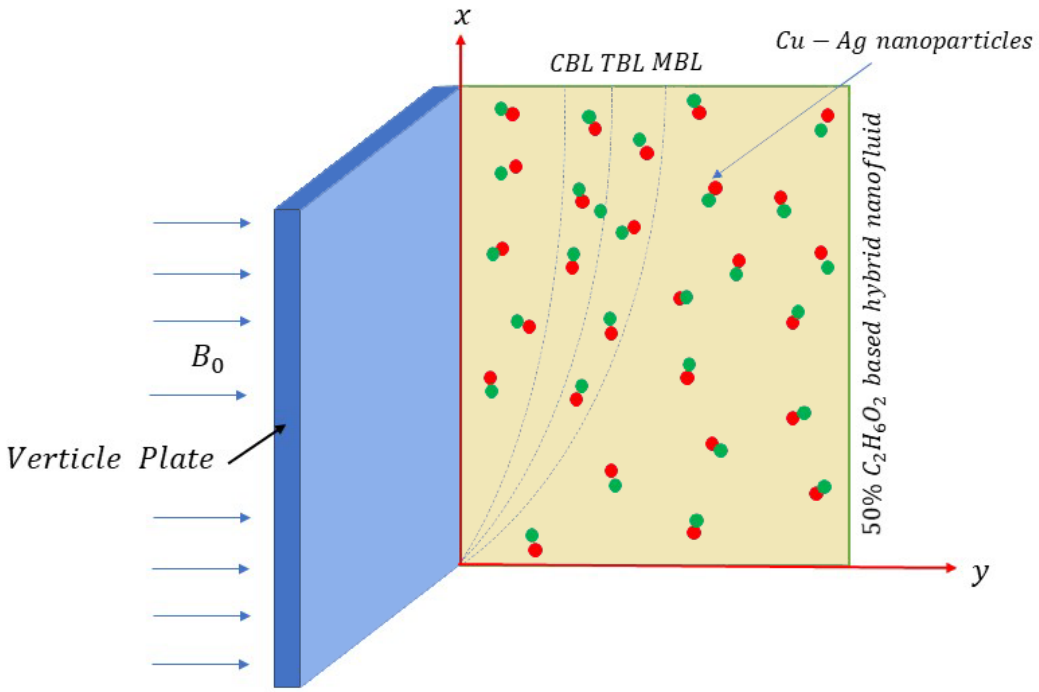

Fig. 1 Flow Geometry and coordinate system.

The corresponding boundary constraints are as follows:

$$y=0: u=U_w, v=0, -k_{hnf}\frac{\partial T}{\partial y}=h_f\left(T_m-T\right), C=C_m \tag{5}$$

$$y\to\infty: u=U_\infty, T=T_\infty, C=C_\infty \tag{6}$$

Dimensionless stream function and similarity coordinate are as follow:

$\psi=\nu_f\sqrt{\mathrm{Re}}\,f(\eta)$, $\eta=\frac{y}{x}\sqrt{\mathrm{Re}}$,

$$u=Uf'(\eta),\ v=\frac{1}{2}\sqrt{\frac{\nu_f U}{x}}\left(\eta f'(\eta)-f(\eta)\right),\ \theta(\eta)=\frac{T-T_\infty}{T_m-T_\infty},\ \chi(\eta)=\frac{C-C_\infty}{C_m-C_\infty},$$

where $U=U_w+U_\infty$. is the composite velocity, ψ is the stream function defined as $u=\frac{\partial\psi}{\partial y}$, $v=-\frac{\partial\psi}{\partial x}$ which identically satisfies Eq. (1). The expressions for ρ_{hnf}, $\left(\rho Cp\right)_{hnf}$, $\left(\rho\beta\right)_{hnf}$, k_{hnf}, μ_{hnf}, D_{hnf} and σ_{hnf} are given by [32,41]:

$$\frac{\rho_{hnf}}{\rho_f}=\left(1-\phi_2\right)\left[\left(1-\phi_1\right)+\phi_1\frac{\rho_{s1}}{\rho_f}\right]+\phi_2\frac{\rho_{s2}}{\rho_f},$$

$$\frac{\left(\rho Cp\right)_{hnf}}{\left(C_p\rho\right)_f}=\left(1-\phi_2\right)\left[\left(1-\phi_1\right)+\phi_1\left(\frac{\left(\rho Cp\right)_{s1}}{\left(\rho Cp\right)_f}\right)\right]+\phi_2\frac{\left(\rho Cp\right)_{s2}}{\left(\rho Cp\right)_f},$$

$$\frac{\left(\rho\beta\right)_{hnf}}{\left(\rho\beta\right)_f}=\left(1-\phi_2\right)\left[\left(1-\phi_1\right)+\phi_1\left(\frac{\left(\rho\beta\right)_{s1}}{\left(\rho\beta\right)_f}\right)\right]+\phi_2\frac{\left(\rho\beta\right)_{s2}}{\left(\rho\beta\right)_f}$$

$$\frac{k_{hnf}}{k_{bf}}=\frac{k_{s_2}+2k_{bf}-2\phi_2\left(k_{bf}-k_{s_2}\right)}{k_{s_2}+2k_{bf}+\phi_2\left(k_{bf}-k_{s_2}\right)},\ \frac{k_{bf}}{k_f}=\frac{k_{s_1}+2k_f-2\phi_1\left(k_f-k_{s_1}\right)}{k_{s_1}+2k_f+\phi_1\left(k_f-k_{s_1}\right)},$$

$$\mu_{hnf}=\frac{\mu_f}{\left(1-\phi_1\right)^{2.5}\left(1-\phi_2\right)^{2.5}},\ D_{hnf}=\left(1-\phi_1\right)^{2.5}\left(1-\phi_2\right)^{2.5}D_f$$

$$\frac{\sigma_{hnf}}{\sigma_{bf}}=\left[\frac{\sigma_{s_2}(1+2\phi_2)+2\sigma_{bf}(1-\phi_2)}{\sigma_{s_2}(1-\phi_2)+\sigma_{bf}\left(2+\phi_2\right)}\right],\frac{\sigma_{bf}}{\sigma_f}=\left[\frac{\sigma_{s_1}(1+2\phi_1)+2\sigma_f(1-\phi_1)}{\sigma_{s1}(1-\phi_1)+\sigma_f\left(2+\phi_1\right)}\right]$$

By using similarity transformations, the equations (2)-(4) are reduced to the following form:

$$\varepsilon_1\left(1+\frac{1}{\beta^*}\right)f'''+\frac{1}{2}ff''-\varepsilon_2\frac{\sigma_{hnf}}{\sigma_f}Mf'+\varepsilon_3gr\theta=0 \tag{7}$$

$$\varepsilon_4\frac{k_{hnf}}{k_f}\left(\frac{1}{Pr}\right)\theta''+\frac{1}{2}f\theta'+\varepsilon_4\frac{\sigma_{hnf}}{\sigma_f}MEc\left[\left(f'\right)^2\right]=0 \tag{8}$$

$$\left(1-\phi_1\right)^{2.5}\left(1-\phi_2\right)^{2.5}\left(\frac{1}{Sc}\right)\chi''+\frac{1}{2}f\chi'-\sigma(1+\delta\theta)^n\exp\left[-\frac{E}{1+\delta\theta}\right]\chi=0 \tag{9}$$

Where,

$$\varepsilon_1=\frac{1}{\left(1-\phi_1\right)^{2.5}\left(1-\phi_2\right)^{2.5}\left[\left(1-\phi_2\right)\left[\left(1-\phi_1\right)+\phi_1\frac{\rho_{s1}}{\rho_f}\right]+\phi_2\frac{\rho_{s2}}{\rho_f}\right]},$$

$$\varepsilon_2=\frac{1}{\left[\left(1-\phi_2\right)\left[\left(1-\phi_1\right)+\phi_1\frac{\rho_{s1}}{\rho_f}\right]+\phi_2\frac{\rho_{s2}}{\rho_f}\right]},$$

$$\varepsilon_3=\frac{\left(1-\phi_2\right)\left[\left(1-\phi_1\right)+\phi_1\left(\frac{\left(\rho\beta\right)_{s1}}{\left(\rho\beta\right)_f}\right)\right]+\phi_2\frac{\left(\rho\beta\right)_{s2}}{\left(\rho\beta\right)_f}}{\left(1-\phi_2\right)\left[\left(1-\phi_1\right)+\phi_1\frac{\rho_{s1}}{\rho_f}\right]+\phi_2\frac{\rho_{s2}}{\rho_f}},$$

$$\varepsilon_4 = \frac{1}{(1-\phi_2)\left[(1-\phi_1)+\phi_1\left(\frac{(\rho Cp)_{s1}}{(\rho Cp)_f}\right)\right]+\phi_2\frac{(\rho Cp)_{s2}}{(\rho Cp)_f}}$$

Corresponding reduced boundary conditions are:

$$f(0)=0,\ f'(0)=m_1,\ \frac{k_{hnf}}{k_f}\theta'(0)=-Bi\left(1-\theta(0)\right),\ \chi(0)=1 \tag{10}$$

$$f'(\infty)=1-m_1,\ \theta(\infty)=0,\ \chi(\infty)=0 \tag{11}$$

The parameters and dimensionless numbers in the above equations are defined as follow: $M=\frac{\sigma_f B_0^2 x}{\rho_f U}$ is magnetic parameter, $Gr=\frac{g\beta_f(T_m-T_\infty)x^3}{\nu_f{}^2}$ is Grashof number, $\mathrm{Re}=\frac{Ux}{\nu_f}$ is Reynolds number, $gr=\frac{Gr}{\mathrm{Re}^2}$ is mixed convection parameter, $Ec=\frac{U^2}{C_p(T_m-T_\infty)}$ is Eckert number, $Pr=\frac{\nu_f(\rho C_p)_f}{k_f}$ is Prandtl number, $Sc=\frac{\nu_f}{D_f}$ is Schmidt number, $\delta=\frac{T_m-T_\infty}{T_\infty}$ is temperature difference, $E=\frac{E_a}{KT_\infty}$ is dimensionless activation energy, $\sigma=\frac{k_r^2 x}{U}$ is chemical reaction rate parameter , $Bi=\frac{h_f}{k_f}\sqrt{\frac{\nu_f x}{U}}$ is Biot number.

The practical interest includes the skin-friction coefficient, Nusselt number and Sherwood number. The dimensionless forms of respective physical quantities are given by:

$$\mathrm{Re}^{1/2}\,C_f=\left(1+\frac{1}{\beta^*}\right)\frac{f''(0)}{(1-\phi_1)^{2.5}(1-\phi_2)^{2.5}} \tag{12}$$

$$\mathrm{Re}^{-1/2}\,Nu=-\frac{k_{hnf}}{k_f}\theta'(0),\ \mathrm{Re}^{-1/2}\,Sh=-(1-\phi_1)^{2.5}(1-\phi_2)^{2.5}\,\chi'(0) \tag{13}$$

3. Numerical Methodology

The set of PDE's are reduced to ODE's by opting appropriate similarity variables with corresponding boundary constraints. To understand the phenomena of the model, the non-linear deferential equations (7)-(9) with corresponding boundary constraints (10)-(11) are solved by using RKF-45 method along with the shooting scheme. As required by the method of lines implemented in this built-in function and also, the reduced equations with corresponding boundary conditions are transformed into the following system of first-order differential equations using the substitution $f=y(1),\ f'=y(2),\ f''=y(3),\ \theta=y(4),\theta'=y(5),\ \chi=y(6)\ and\ \chi'=y(7)$. The calculations have been carried out for several values of the formerly defined parameters. This routine is based on the standard shooting technique with fourth order Runge–Kutta process. We hand-picked an apt finite value of η_∞ so that far field boundary constraints are satisfied asymptotically. A limited

domain in η -direction can be used instead with η selected large enough to ensure that the solutions are not affected by placing asymptotic conditions at a limited range. In this present study, a suitable finite value of η_∞ is considered as $\eta_\infty < 11$ in such way that not only numerical solutions converge but also boundary conditions defined at infinity satisfy asymptotically. The comparative error tolerance 10^{-6} is well-thought-out for convergence and the step size is selected as $\Delta\eta = 0.001$. Further the CPU time to estimate the velocity values (1.38sec) is much fewer than the CPU time to evaluate the temperature values (1.56 sec) and the CPU time for concentration is 2.05 sec.

4. Results and Discussions

This section is dedicated to inspect the aspects of physical parameters that influence the performance of velocity, temperature, and concentration fields. Also, a variation of skin friction, Nusselt number, and Sherwood number is analyzed graphically. The Prandtl number value is set for 20.1 at room temperature and the volume fraction is kept constant at 0.02. RKF-45 technique is one of the most suitable technique to find the numerical approximations to non-linear ODE's. On-going through plotted figures we detected a very good agreement in the results obtained by RKF-45 method by adopting shooting technique with previously published results. For a check, we also compared obtained numerical results with the published work. Table.1 is constructed for comparative values of present results with existing work and obtained a good agreement with each other. The thermophysical properties of nanoparticles are mentioned in Table.2. (Refer Gholinia et al. [33] and Ghadikolaei and Gholinia [34] for physical properties).

Table 1: Comparison Values of $f''(0)$ without mass transfer when $\epsilon_1 = \left(1 + \frac{1}{\beta^*}\right) = \epsilon_4 = \frac{k_{hnf}}{kf} = 1$ and $\epsilon_2 = \epsilon_3 = M = 0$.

Author(s)	$m_1 = 0$	$m_1 = 1$
Blasius [35]	0.332	-
Sakiadis [36]	-	-0.44375
Ishak et al. [37]	0.3321	-0.4438
Bachok et al. [38]	0.3321	-0.4438
Anuar et al. [39]	0.3321	-0.4438
Anuar et al. [40]	0.332057	-0.443751
Present results	0.3320822314298	-0.4438321677931

Table.2: Thermophysical properties of Ethylene glycol, silver and copper nanoparticles

Physical properties	50% $C_2H_6O_2$	Ag	Cu
ρ	1063.8	10500	8933
k	0.387	0.613	400

C_p	3630	253	385
σ	9.75×10^{-4}	6.30×10^{7}	5.96×10^{7}
β	5.8×10^{-5}	1.89×10^{-5}	1.67×10^{-5}

4.1 Influence of parameters on velocity profile:

Fig. 2 portrays the deviation in dimensionless velocity gradient with the impact of Casson parameter β^*. It is noticed that inclination in β^* declines the velocity gradient in vertically moving plate but opposite behaviour can be observed for the flow with $m_1 = 0$. Incline in β^* declines the values of yield stress and reduces the passage rate. So that the boundary layer thickness of vertically moving plate declines. The influence of M on velocity gradient for both the flows in motionless surface with an unvarying free stream velocity $m_1 = 0$ and vertically moving plane surface moving in a stagnant free stream $m_1 = 1$ is displayed in Fig. 3. The flow of nanofluid is reduced by the resistive force also called as Lorentz force raised by the magnetic field. The viscous forces get overriding in this case. Hence, the fluid velocity declines and it reduces the thickness of the related boundary layer of both Sakiadis and Blasius flow. The effect of gr on fluid velocity is shown in Fig. 4. The increase in Grashof number enhances the buoyancy or mixed convection parameter. One can detect from the figure that, inclination in gr upsurges the velocity of the fluid in a motion and boundary layer thickness related to f'. The increasing buoyancy forces upsurges the nanofluid flow of fractional nanofluids which enhances the fluid velocity in stationary surface with an unvarying free stream velocity $m_1 = 0$ and vertically moving plane surface in a stagnant free stream $m_1 = 1$.

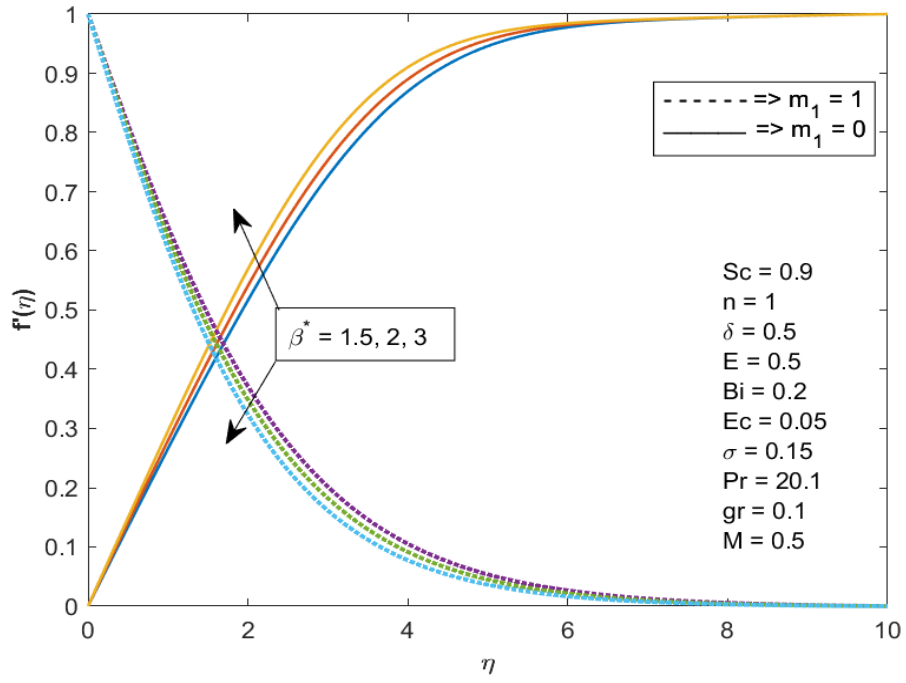

Fig. 2 Effect of β^* on $f'(\eta)$

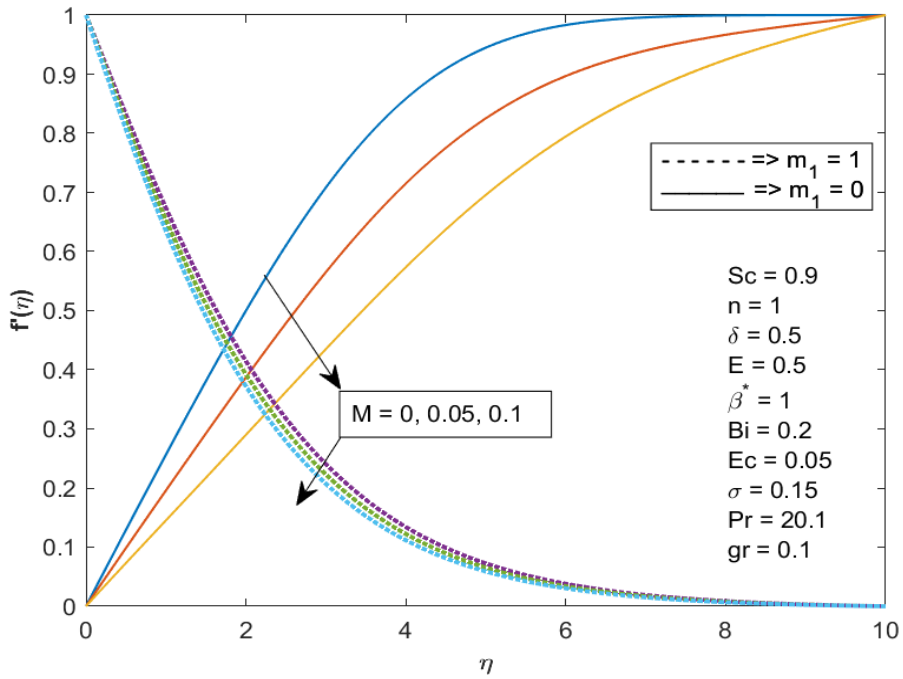

Fig. 3 Effect of M on $f'(\eta)$

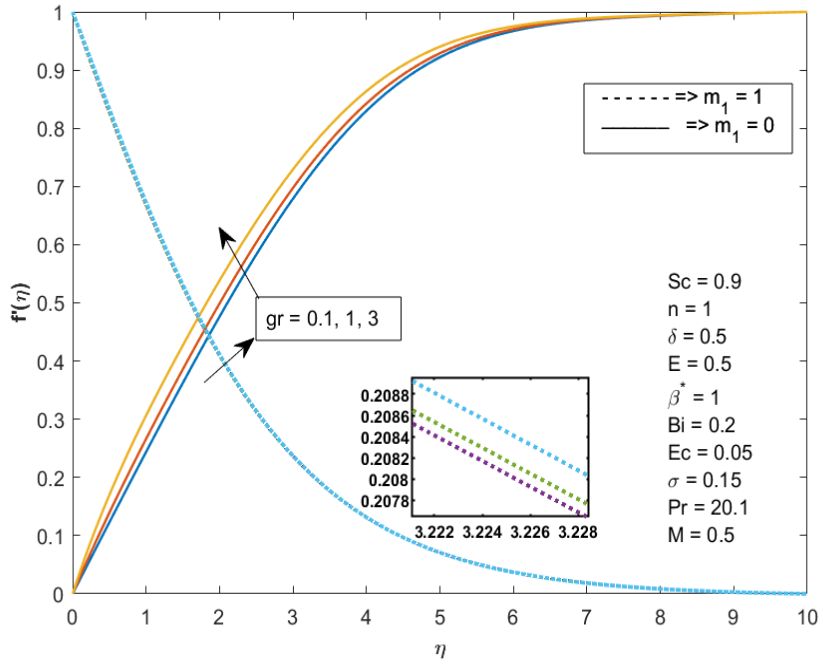

Fig. 4 Impact of gr on $f'(\eta)$

4.2 Influence of parameters on Thermal profile:

The impact of M on thermal profile is exemplified in Fig.5. It is seen from Fig.5 that growth in M enriches the thermal profile in both the fluid flow representing Blasius and Sakiadis flow. Increasing in Magnetic parameter intensify the magnetic field. Here, the temperature of the liquid gradually increases due to joule heating which supplies the additional heat to the flow system, which results in enhancing thermal gradient and related boundary layer thickness in stationary surface with a uniform free stream velocity $m_1 = 0$ and vertically moving plane surface moving in a stagnant free stream $m_1 = 1$. Fig .6 illustrates the influence of Pr on thermal profile. Pr number is set as 11.8, 8.3, 6.6, for 50% of Ethylene Glycol by rising the temperature to 60, 80, and 100 ^{0}C respectively. We observed from Fig .6 that rise in Prandtl number declines the thermal profile. Fluids possess higher thermal conductivities for lower Prandtl numbers, so that in this circumstances heat can diffuse from the plate quicker than in liquids with inclined Pr. Identical behaviour can be observed in both the fluid flow with $m_1 = 0$ and $m_1 = 1$. Fig. 7 portrays the impact of Eckert number on thermal gradient representing both Blasius and Sakiadis flow. It is detected from figure that, rise in Ec enhances the thermal profile. It is moderately clear from the description of Ec that its higher values give rise to the strong Ohmic effect, which upsurges the temperature and its related boundary layer thickness. Hence, increase in Ec enhances the temperature gradients in stationary surface with a uniform free stream velocity $m_1 = 0$ and vertically moving plane surface moving in a stagnant free stream $m_1 = 1$. Fig.8 indicates the impact of Bi on thermal profile. Increase in Biot number boost ups the thermal gradient. Also, it is detected that a small change in the Bi has significant role in temperature enhancement. Inclining value of Bi shoot-ups the thermal gradient for both the flows with $m_1 = 0$ and $m_1 = 1$.

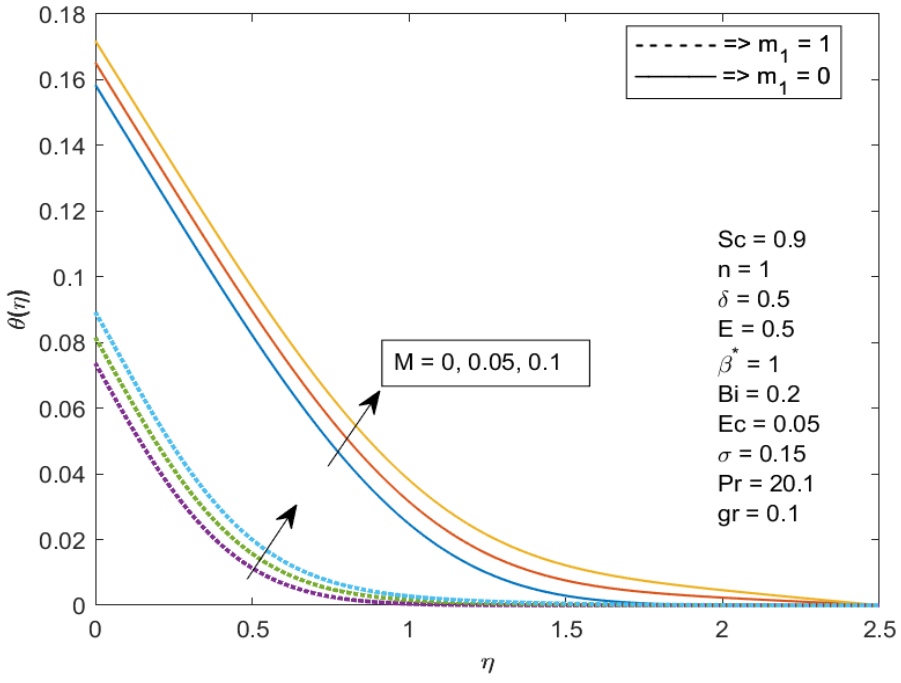

Fig. 5 Effect of M on $\theta(\eta)$

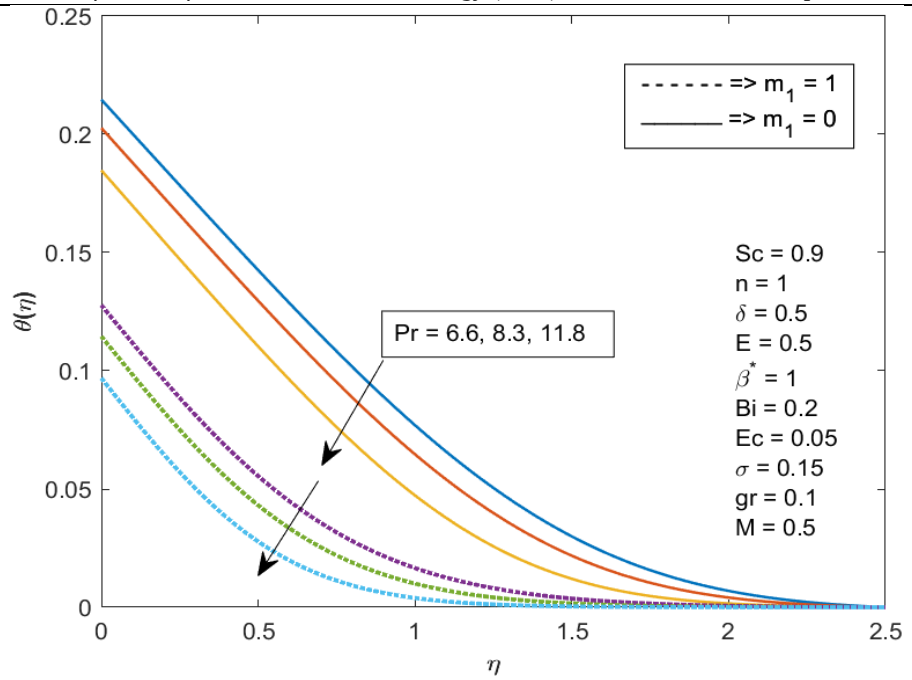

Fig. 6 Effect of Pr on $\theta(\eta)$

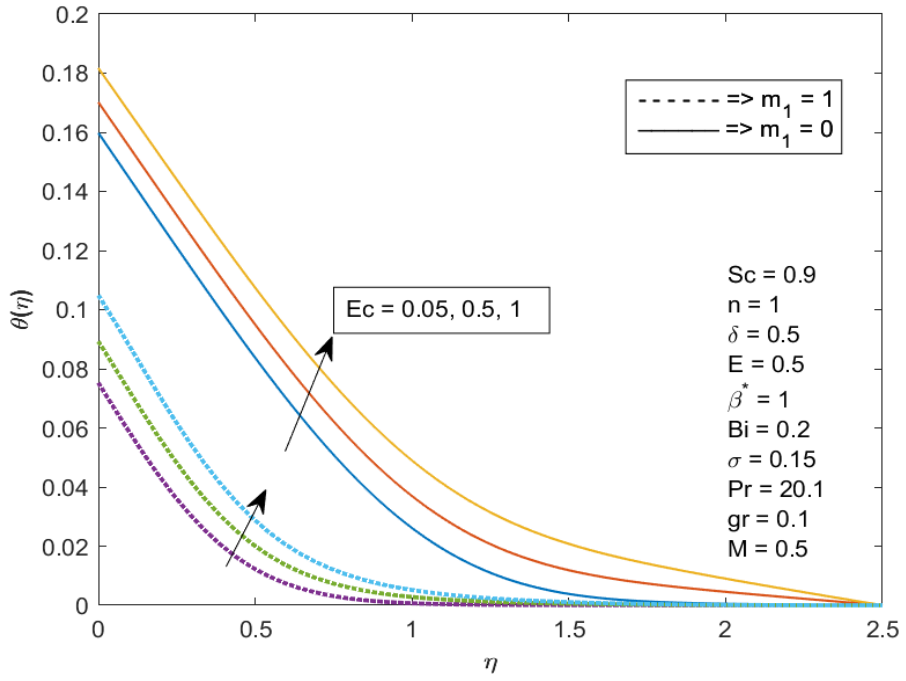

Fig. 7 Influence of *Ec* on $\theta(\eta)$

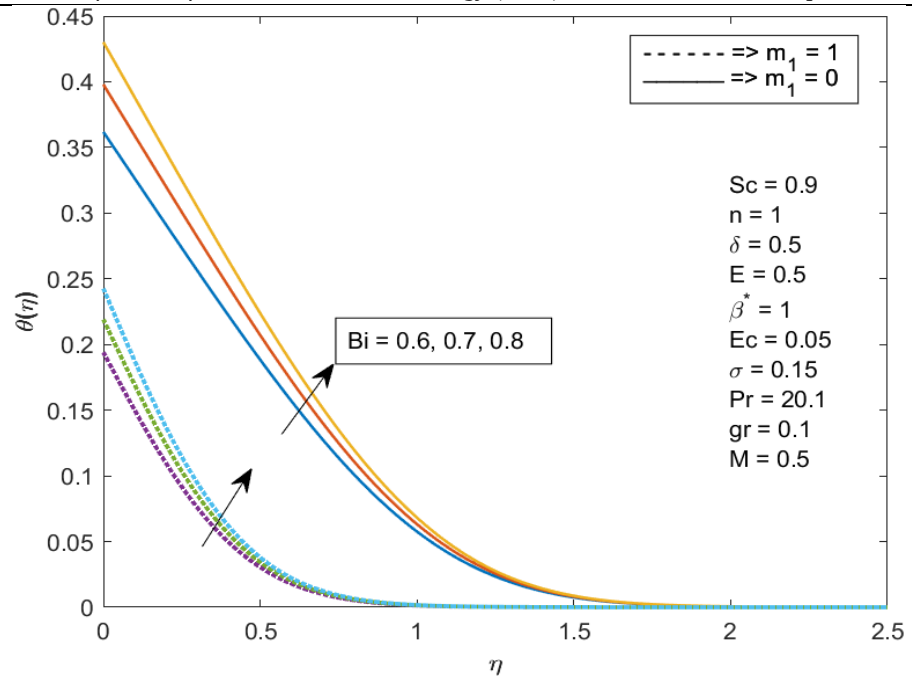

Fig. 8 Impact of Bi on $\theta(\eta)$

4.3 Influence of parameters on Concentration profile:

Consequence of magnetic parameter on concentration gradient is demonstrated in Fig. 9. It shows that rise in M enhances the concentration profile. In fact, the Lorentz force declares that the induced magnetic field declines the fluid motion which inclines the concentration gradient. Identical variation in concentration gradient can be observed for both the flows representing Blasius and Sakiadis flow. Fig. 10 is plotted to analyse the influence of Sc on concentration gradient for both Blasius and Sakiadis flow. It is detected from figure that increase in values of Sc diminishes the concentration profile. Physically, the rise in values of Sc reasons for lessening in molecular diffusivity of the fluid which enhances the concentration of both the flows. Fig.11 portrays an instance of change in concentration gradient for several values of σ. It can be seen from Fig that rise in σ declines the concentration profile. Upsurge in σ improves the volume fraction of nanoparticles. Here, concentration profile has insufficient power of buoyancy forces, which causes the deteriorating behaviour of nanoparticle concentration in flow representing both Blasius and Sakiadis flow. The impact of E on χ versus η is displayed in Fig.12. It is noted that increase in activation energy boost ups the $\chi(\eta)$. It is obvious that increase in E enhances the concentration of nanoparticle and connected layer thickness. Hence, the upsurge in values of E inclines the concentration profile of both the flows with $m_1 = 0$ and $m_1 = 1$.

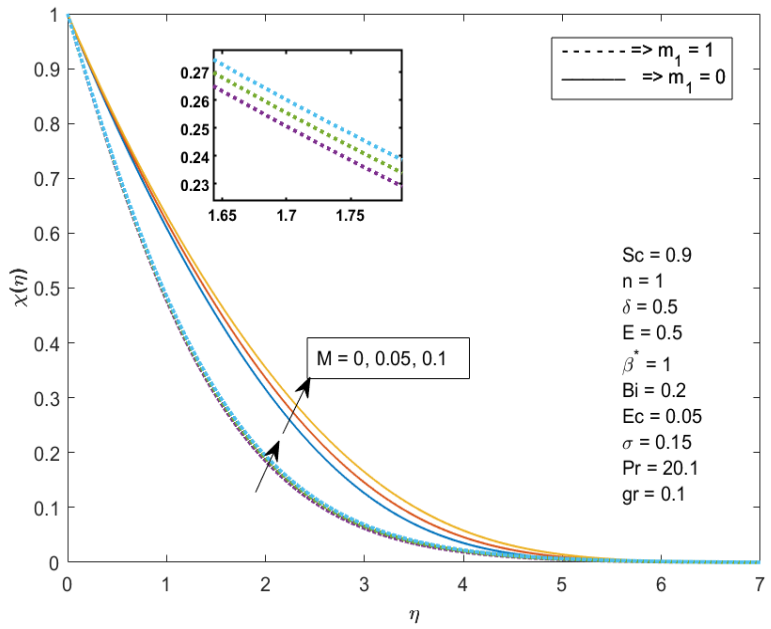

Fig. 9 Impact of M on $\chi(\eta)$

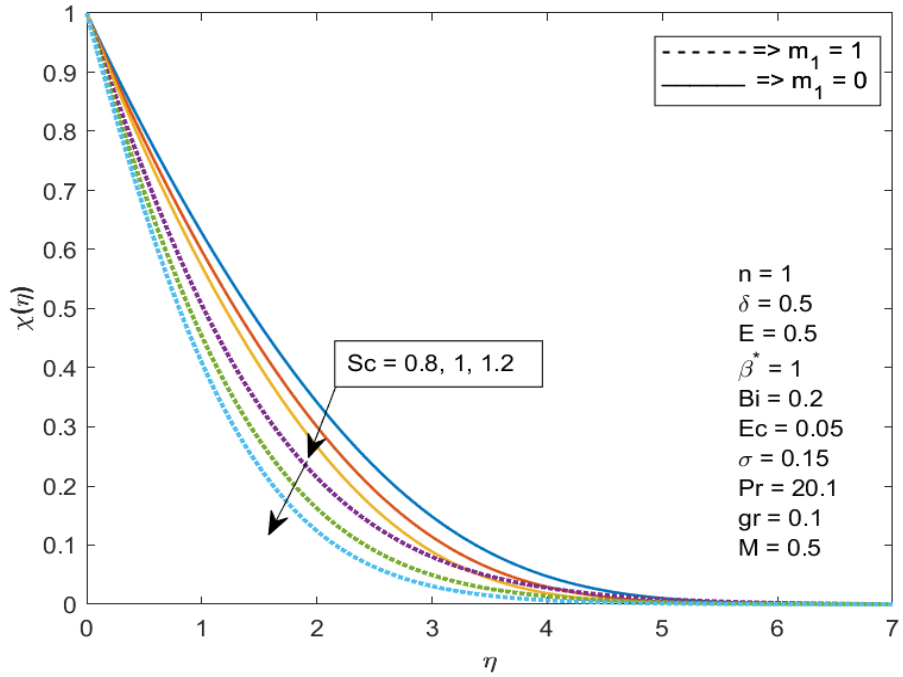

Fig. 10 Impact of *Sc* on $\chi(\eta)$

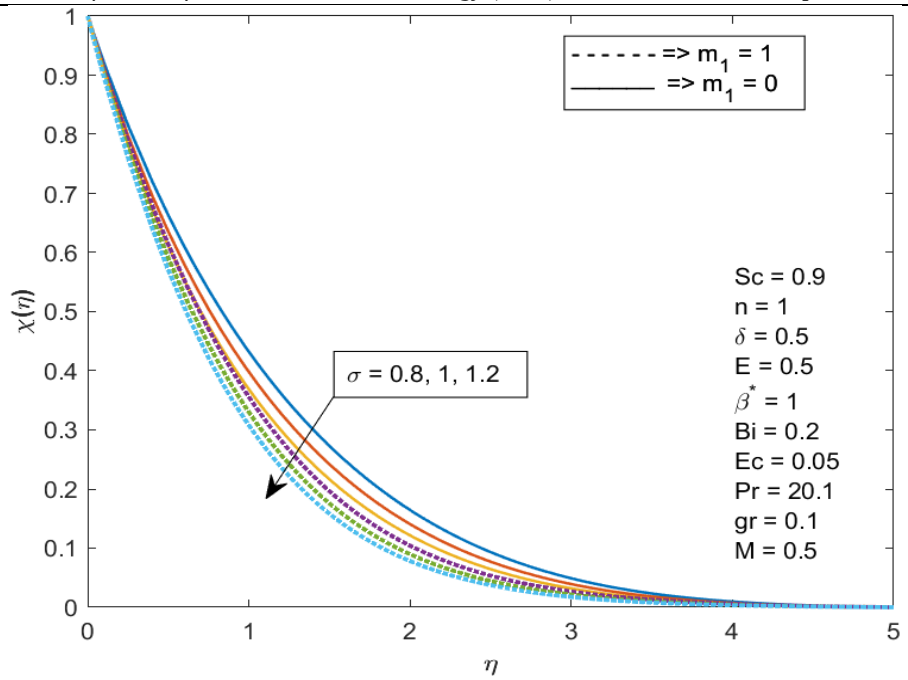

Fig. 11 Impact of σ on $\chi(\eta)$

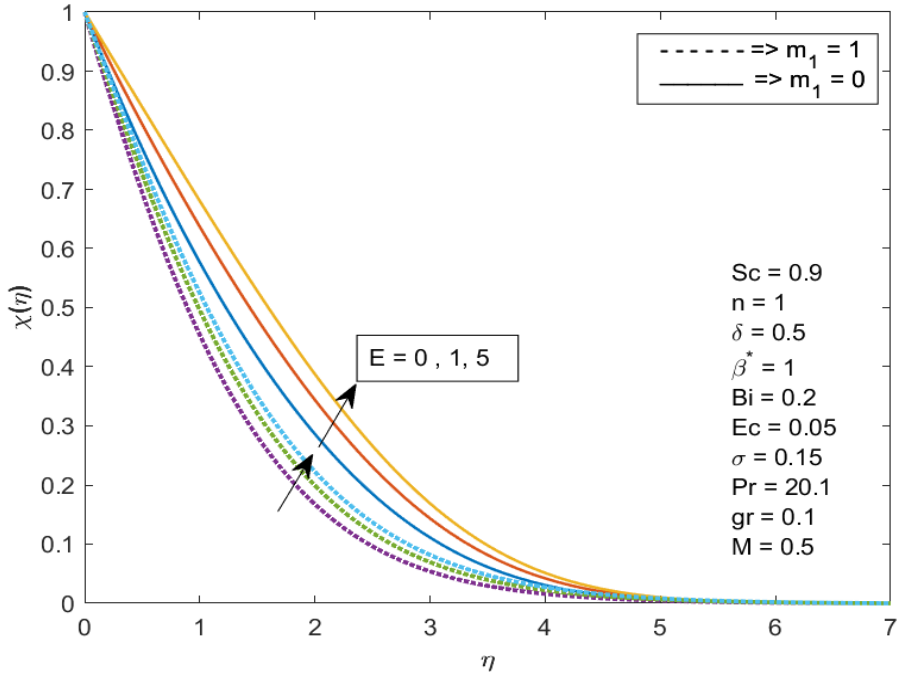

Fig. 12 Impact of E on $\chi(\eta)$

4.4 Influence of parameters on Skin friction, Nusselt and Sherwood numbers:

Fig.13 shows the sway of β^* on $\mathrm{Re}^{1/2} C_f$. It is detected from plot that inclination in β^* with respect to upsurge in M declines the $\mathrm{Re}^{1/2} C_f$ of both the flows. It is noted from the Fig that, the rate of declining is faster in Blasius flow when related to Sakiadis flow. Fig. 14 illustrates the impact of Bi on $\mathrm{Re}^{-1/2} Nu$ versus Ec. One can see from Fig.14 that upsurge in Bi with respect to inclined Ec inclines the Nusselt number of the both Blasius and Sakiadis flow. It is also noted that increase in rate of heat transfer is slower in Blasius than Sakiadis flow. Impact of Sc on $\mathrm{Re}^{-1/2} Sh$ by varying E representing Blasius and Sakiadis flow is portrayed in Fig. 15. $\mathrm{Re}^{-1/2} Sh$ gradually decreases with inclination in E with respect to Sc . Rate of mass transfer is quite faster in Sakiadis flow when compared to Blasius flow.

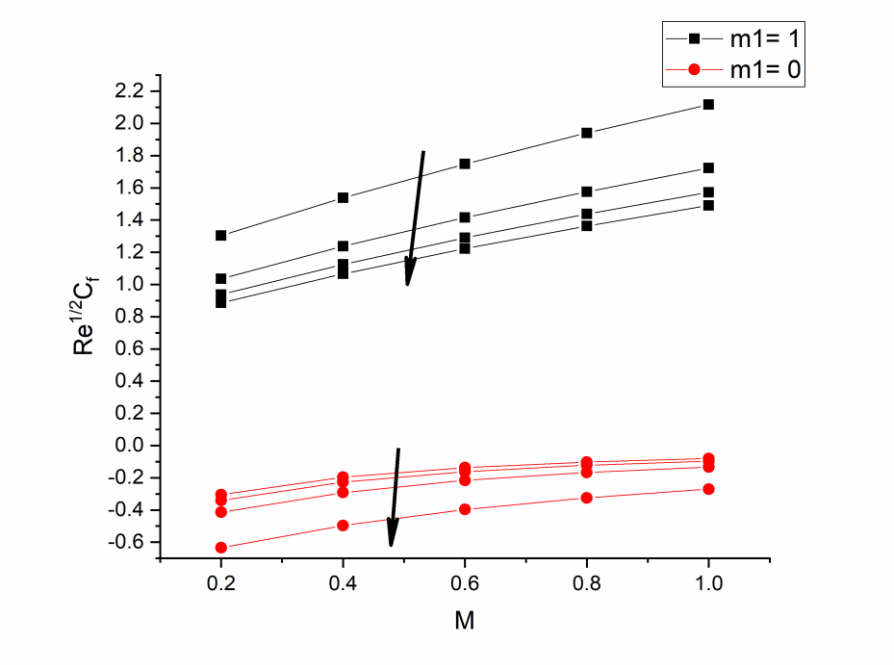

Fig. 13 Change in pattern of $\mathrm{Re}^{1/2} C_f$ over M by varying $\beta^* (= 0.5, 1, 1.5, 2)$

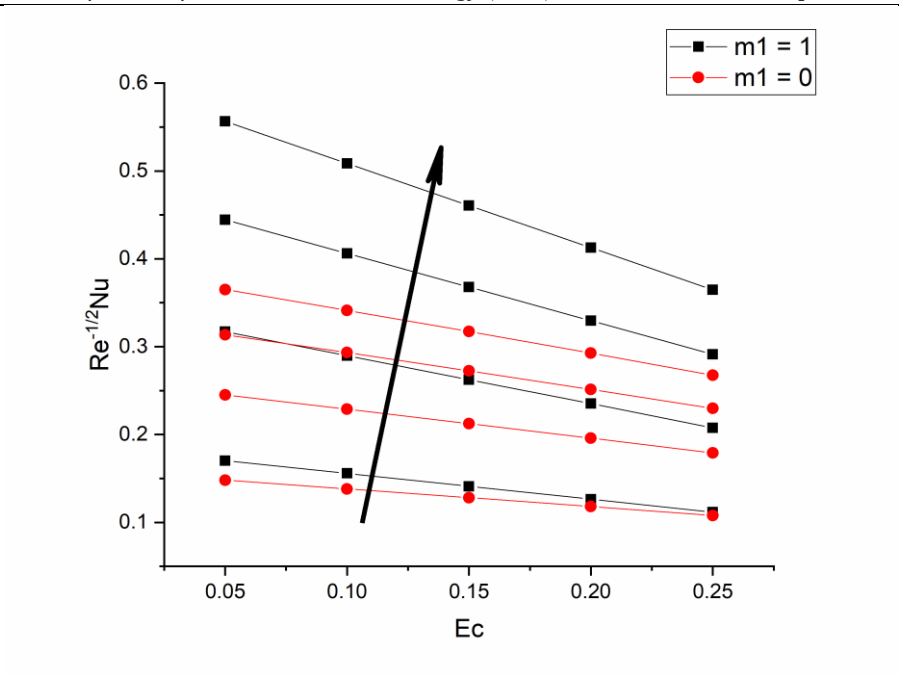

Fig. 14 Change in pattern of $\mathrm{Re}^{-1/2}\,Nu$ over Ec by varying $Bi = (0.2, 0.4, 0.6, 0.8)$

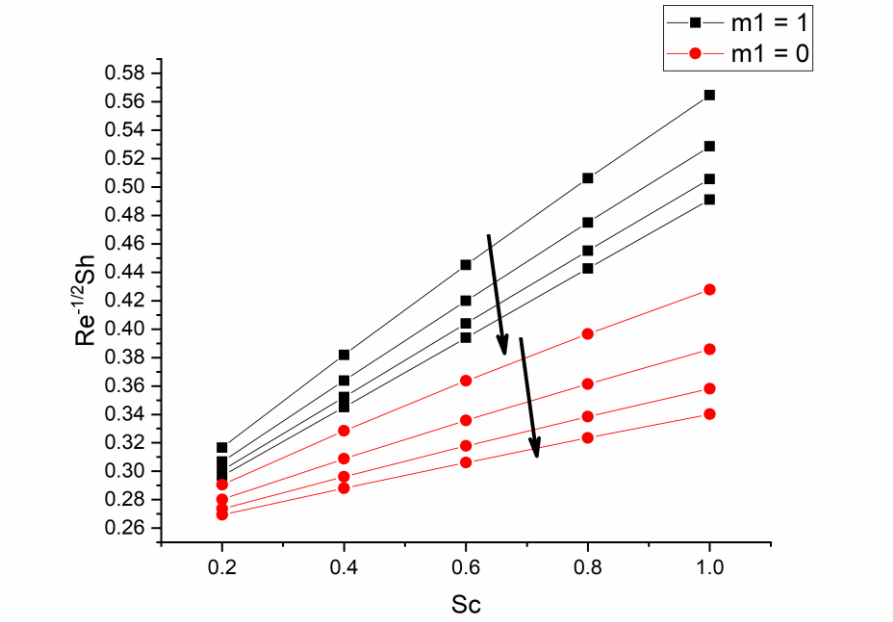

Fig. 15 Change in pattern of $\mathrm{Re}^{-1/2}\,Sh$ over Sc by varying $E(= 0.5, 1, 1.5, 2)$

5. Conclusion

In the current analysis, Blasius and Sakiadis flow of a Casson hybrid nanofluid over a moving plate with convective boundary constraint, activation energy and Joule heating is examined. Here, we have considered 50% of Ethylene glycol as base fluid with Silver and

copper nanoparticles. The system of PDE's is modified into ODE's by using the similarity variables. The reduced ODE's are resolved numerically with the assistance of RKF-45 method by adopting shooting technique. The implications of pertinent constraints on fluid fields are explicated with the aid of graphs. Some of the significant outcomes are as follows:

- Rise in values of Casson parameter reduces the velocity gradient in vertically moving plate and inclines the velocity of fluid flow in stationary surface with a uniform free stream.
- Increase in magnetic parameter declines velocity gradient but strengthen the thermal and concentration gradient in both the flows of fluid.
- Enhance in gr progresses the velocity gradient in both the flows.
- Increase in Pr at different temperature diminishes the thermal profile representing both Blasius and Sakiadis.
- Rise in values of Eckert and Biot numbers upsurges the thermal gradient in stationary surface with a uniform free stream velocity $m_1 = 0$ and vertically moving plane surface moving in a stagnant free stream $m_1 = 1$.
- Upsurge in reaction rate declines concentration gradient in both the flow representing Blasius and Sakiadis flow.
- Inclined values of activation energy upsurge the concentration gradient in stationary surface with an unvarying free stream velocity and vertically moving plane surface in a stagnant free stream.

References

[1] S.U.S. Choi, Enhancing thermal conductivity of fluids with nanoparticles, ASME Fluids Eng. Division, 231 (1995) 99–105.

[2] S. Hoseinzadeh, S. A. R. Sahebi, R. Ghasemiasl, and A. R. Majidian, Experimental analysis to improving thermosyphon (TPCT) thermal efficiency using nanoparticles/based fluids (water), Eur. Phys. J. Plus, 132 (2017) 197.

[3] M. Sheikholeslami, H. B. Rokni, Effect of melting heat transfer on nanofluid flow in existence of magnetic field considering Buongiorno Model, Chin. J. Phys. 55 (2017) 115–1126.

[4] S. Hoseinzadeh, S. M. T. Otaghsara, M. H. Z. Khatir, P. S. Heyns, Numerical investigation of thermal pulsating alumina/water nanofluid flow over three different cross-sectional channel, Int. J. Numer. Methods Heat Fluid Flow. 30 (2019) 3721–3735.

[5] M. Ijaz Khan, A. Alsaedi, S. Qayyum, T. Hayat, M. Imran Khan, Entropy generation optimization in flow of Prandtl–Eyring nanofluid with binary chemical reaction and Arrhenius activation energy, Colloids Surf. Physicochem. Eng. Asp. 570 (2019) 117–126.

[6] S. Hoseinzadeh, P. S. Heyns, H. Kariman, Numerical investigation of heat transfer of laminar and turbulent pulsating Al2O3/water nanofluid flow, Int. J. Numer. Methods Heat Fluid Flow. 30 (2020) 1149–1166.

[7] H. B. Mallikarjuna, T. Nirmala, R. J. P. Gowda, R. Manghat, R. S. V. Kumar, Two-dimensional Darcy–Forchheimer flow of a dusty hybrid nanofluid over a stretching sheet with viscous dissipation, Heat Transf. (2020).

[8] R. J. Punith Gowda, R. Naveen Kumar, Ali Aldalbahi, Alibek Issakhov, B. C. Prasannakumara, Mohammad Rahimi-Gorji, Mostafizur Rahman, Thermophoretic particle deposition in time-dependent flow of hybrid nanofluid over rotating and vertically upward/ downward moving disk, Surfaces and Interfaces. 22 (2020) 100864.

[9] G. Rasool, A. J. Chamkha, T. Muhammad, A. Shafiq, and I. Khan, Darcy-Forchheimer relation in Casson type MHD nanofluid flow over non-linear stretching surface, Propuls. Power Res., 9 (2020) 159–168.

[10] M. Amjad, I. Zehra, S. Nadeem, N. Abbas, Thermal analysis of Casson micropolar nanofluid flow over a permeable curved stretching surface under the stagnation region, J. Therm. Anal. Calorim. 143 (2020) 2485–2497.

[11] W. Jamshed, A. Aziz, Cattaneo–Christov based study of TiO 2 –CuO/EG Casson hybrid nanofluid flow over a stretching surface with entropy generation, Appl. Nanosci. 8 (2018) 685–698.

[12] S. Aman, S. M. Zokri, Z. Ismail, M. Z. Salleh, I. Khan, Effect of MHD and porosity on exact solutions and flow of a hybrid casson-nanofluid, J. Adv. Res. Fluid Mech. Therm. Sci. 44 (2018) 131–139.

[13] S. Ahmad, S. Nadeem, Cattaneo–Christov-based study of SWCNT–MWCNT/EG Casson hybrid nanofluid flow past a lubricated surface with entropy generation, Appl. Nanosci.10 (2020) 5449–5458.

[14] B. C. Prasannakumara, B. J. Gireesha, P. T. Manjunatha, Melting Phenomenon in MHD Stagnation Point Flow of Dusty Fluid over a Stretching Sheet in the Presence of Thermal Radiation and Non-Uniform Heat Source/Sink, Int. J. Comput. Methods Eng. Sci. Mech. 16 (2015) 265–274.

[15] M. Ramzan, J. D. Chung, N. Ullah, Partial slip effect in the flow of MHD micropolar nanofluid flow due to a rotating disk – A numerical approach, Results Phys. 7 (2017) 3557–3566.

[16] B. C. Prasannakumara, B. J. Gireesha, M. R. Krishnamurthy, R. S. R. Gorla, Slip flow and nonlinear radiative heat transfer of suspended nanoparticles due to a rotating disk in the presence of convective boundary condition, Int. J. Nanoparticles. 9 (2017) 180–200.

[17] M. Khan, M. Azam, Unsteady heat and mass transfer mechanisms in MHD Carreau nanofluid flow, J. Mol. Liq.225 (2017) 554–562.

[18] B. C. Prasannakumara, B. J. Gireesha, M. R. Krishnamurthy, K. Ganesh Kumar, MHD flow and nonlinear radiative heat transfer of Sisko nanofluid over a nonlinear stretching sheet, Inform. Med. Unlocked. 9 (2017) 123–132.

[19] A. J. Christopher, N. Magesh, R. J. P. Gowda, R. N. Kumar, R. S. V. Kumar, Hybrid nanofluid flow over a stretched cylinder with the impact of homogeneous–heterogeneous reactions and Cattaneo–Christov heat flux: Series solution and numerical simulation, Heat Transf. (2020).

[20] M. Ahmad, F. Jalil, M. Taj, S. A. Shehzad, Lubrication aspects in an axisymmetric magneto nanofluid flow with radiated chemical reaction, Heat Transf. 49 (2020) 3489–3502.

[21] A. Tulu, W. Ibrahim, Spectral relaxation method analysis of Casson nanofluid flow over stretching cylinder with variable thermal conductivity and Cattaneo–Christov heat flux model, Heat Transf. 49 (2020) 3433–3455.

[22] S. Mishra, A. Misra, M. Nayak, Flow and heat transfer of Oldroyd-B nanofluid with relaxation-retardation viscous dissipation and hyperbolic boundary conditions, Int. J. Thermofluid Sci. Technol. 7 (2020) 20070104.

[23] M. J. Kotresh, G. K. Ramesh, V. K. R. Shashikala, B. C. Prasannakumara, Assessment of Arrhenius activation energy in stretched flow of nanofluid over a rotating disc, Heat Transf. (2020).

[24] M. Ijaz, M. Yousaf, A. M. El Shafey, Arrhenius activation energy and Joule heating for Walter-B fluid with Cattaneo–Christov double-diffusion model, J. Therm. Anal. Calorim. 143 (2020) 3687–3698.

[25] P. Gowda, R. Jayadevamurthy, N. Rangaswamy, Emphasis on unsteady dynamics of bioconvective hybrid nanofluid flow over an upward – downward moving rotating disk, Numer Methods Partial Differential Eq. (2020)1-22.

[26] K. Ganesh Kumar, A. Baslem, B. C. Prasannakumara, J. Majdoubi, M. Rahimi-Gorji, S. Nadeem, Significance of Arrhenius activation energy in flow and heat transfer of tangent hyperbolic fluid with zero mass flux condition, Microsyst. Technol. 26 (2020) 2517–2526.

[27] K. Ganesh Kumar, A. J. Chamkha, B. C. Prasannakumara, A. M. Jyothi, Exploration of particle shape effect on Cu-H2O nanoparticles over a moving plate: An approach of dual solution, Int. J. Numer. Methods Heat Fluid Flow. 30 (2019) 1867–1879.

[28] O. D. Makinde, B. C. P. Kumara, G. K. Ramesh, B. J. Gireesha, Simultaneous Convection of Carreau Fluid with Radiation Past a Convectively Heated Moving Plate, Defect Diffus. Forum. 389 (2018) 60–70.

[29] T. Anwar, P. Kumam, Z. Shah, W. Watthayu, P. Thounthong, Unsteady radiative natural convective MHD nanofluid flow past a porous moving vertical plate with heat source/sink, Molecules. 25 (2020) 1–21.

[30] M. Shuaib, A. Ali, M. A. Khan, A. Ali, Numerical investigation of an unsteady nanofluid flow with magnetic and suction effects to the moving upper plate, Adv. Mech. Eng. 12 (2020) 1–13.

[31] N. S. Anuar, N. Bachok, N. M. Arifin, H. Rosali, Role of multiple solutions in flow of nanofluids with carbon nanotubes over a vertical permeable moving plate, Alexandria Eng. J. 59 (2020) 763–773.

[32] S. Das, R. N. Jana, O. D. Makinde, MHD Flow of Cu-Al2O3/Water Hybrid Nanofluid in Porous Channel: Analysis of Entropy Generation, Defect Diffus. Forum. 377 (2017) 42–61.

[33] M. Gholinia, S. Gholinia, K. Hosseinzadeh, D. D. Ganji, Investigation on ethylene glycol Nano fluid flow over a vertical permeable circular cylinder under effect of magnetic field, Results Phys. 9 (2018) 1525–1533.

[34] S. S. Ghadikolaei, M. Gholinia, Terrific effect of H2 on 3D free convection MHD flow of C2H6O2H2O hybrid base fluid to dissolve Cu nanoparticles in a porous space considering the thermal radiation and nanoparticle shapes effects, Int. J. Hydrogen Energy. 44 (2019) 17072–17083.

[35] H. Blasius, Grenzschichten in Flussigkeiten mit kleiner Reibung, 2. angew, Math. Phye. 56 (1908).

[36] B. C. Sakiadis, Boundary-layer behavior on continuous solid surfaces: I. Boundary-layer equations for two-dimensional and axisymmetric flow, AIChE J. 7 (1961) 26–28.

[37] A. Ishak, R. Nazar, I. Pop, Flow and heat transfer characteristics on a moving flat plate in a parallel stream with constant surface heat flux, Heat Mass Transf. 45 (2009) 563–567.

[38] N. Bachok, A. Ishak, I. Pop, Flow and heat transfer characteristics on a moving plate in a nanofluid, Int. J. Heat Mass Transf. 55 (2012) 642–648.

[39] N. S. Anuar, N. Bachok, I. Pop, A Stability Analysis of Solutions in Boundary Layer Flow and Heat Transfer of Carbon Nanotubes over a Moving Plate with Slip Effect, Energies. 11 (2018) 3243.

[40] N. S. Anuar, N. Bachok, N. M. Arifin, H. Rosali, Role of multiple solutions in flow of nanofluids with carbon nanotubes over a vertical permeable moving plate, Alexandria Eng. 59 (2020) 763–773.

[41] M. Radhika, R. J. P. Gowda, R. Naveenkumar, Siddabasappa, and B. C. Prasannakumara, 'Heat transfer in dusty fluid with suspended hybrid nanoparticles over a melting surface', Heat Transf., (2020).